Check for updates

JGR Atmospheres

RESEARCH ARTICLE
10.1029/2026JD046935

Overestimation of Cloud Sensitivity in Orographic Clouds Over the Southern Tibetan Plateau Due To Neglected Dynamical Constraints

Yuan Wang[1], Fang Fang[1], Jiming Li[1], Ping Zhang[1], Zhao Ji[1], Hailing Jia[2], and Jianping Huang[1]

[1]Collaborative Innovation Center for Western Ecological Safety, College of Atmospheric Sciences, Lanzhou University, Lanzhou, China, [2]SRON Space Research Organisation Netherlands, Leiden, the Netherlands

Key Points:

- Cloud sensitivity follows a sigmoid relationship with increasing cloud-base updraft velocity
- The pattern stems from Köhler theory and its math definition, suggesting potential cross-regime applicability yet needing further validation
- Neglecting dynamical constraints yields a 14%–40% overestimation of the cloud sensitivity for STP orographic clouds

Supporting Information:

Supporting Information may be found in the online version of this article.

Correspondence to:

J. Li,
lijiming@lzu.edu.cn

Citation:

Wang, Y., Fang, F., Li, J., Zhang, P., Ji, Z., Jia, H., & Huang, J. (2026). Overestimation of cloud sensitivity in orographic clouds over the southern Tibetan Plateau due to neglected dynamical constraints. *Journal of Geophysical Research: Atmospheres*, *131*, e2026JD046935. https://doi.org/10.1029/2026JD046935

Received 18 MAR 2026
Accepted 4 OCT 2026

Author Contributions:

Conceptualization: Yuan Wang, Jiming Li
Data curation: Fang Fang, Ping Zhang, Zhao Ji
Formal analysis: Yuan Wang, Fang Fang, Jiming Li, Ping Zhang, Zhao Ji, Hailing Jia
Funding acquisition: Yuan Wang, Jiming Li, Jianping Huang
Investigation: Yuan Wang, Fang Fang
Methodology: Yuan Wang
Project administration: Jianping Huang
Resources: Jiming Li
Supervision: Jiming Li
Validation: Yuan Wang, Ping Zhang, Hailing Jia
Visualization: Ping Zhang
Writing – original draft: Yuan Wang, Fang Fang, Jiming Li

© 2026. American Geophysical Union. All rights reserved, including rights for text and data mining and training of artificial intelligence technologies or similar technologies.

Abstract Accurately quantifying cloud sensitivity (S_{aci}), the relative change in cloud droplet number with aerosol loading, is essential for reducing uncertainties in aerosol–cloud interactions. However, its dependence on cloud dynamics is often overlooked, causing biases in estimates of S_{aci} and Twomey effect radiative forcing (RF_{aci}). Using in situ observations of orographic clouds over the southern Tibetan Plateau (STP), we estimate cloud-base updraft velocity (w) from the water vapor supersaturation budget and examine how S_{aci} varies with w. Results reveal that S_{aci} follows a sigmoid pattern with increasing w. Driven by Köhler activation theory and its mathematical definition, this pattern is theoretically expected to potentially hold across diverse cloud regimes. Ignoring this dependence yields a 14%–40% overestimate of S_{aci} for STP shallow orographic clouds, which may consequently bias local estimates of RF_{aci}. These findings provide new insights into quantifying cloud sensitivity, while their global applicability and implications require further observational validation.

Plain Language Summary Understanding how aerosols affect clouds is important for quantifying climate impacts from aerosol–cloud interactions, but large uncertainties remain. This study focuses on cloud sensitivity, an indicator of how cloud droplet numbers respond to aerosol changes. Using field data from the southern Tibetan Plateau (STP) and a cloud model, we found that cloud sensitivity strongly depends on cloud-base updraft velocity. When this dependence is ignored, cloud sensitivity can be overestimated and may consequently overestimate the calculated radiative forcing from aerosol–cloud interactions in STP orographic clouds. Our results suggest that accounting for this dynamic factor is essential for improving estimates of how aerosols influence Earth's energy balance.

1. Introduction

Aerosol–cloud interactions remain the largest uncertainty in current estimates of anthropogenic radiative forcing (IPCC, 2021). One of the effective ways to reduce this uncertainty is to accurately quantify cloud sensitivity (S_{aci}), defined as the relative change in cloud droplet number concentration (N_C) with respect to aerosol number concentration (N_a),

$$S_{aci} = \frac{d\ln N_C}{d\ln N_a} \quad (1)$$

S_{aci} is a key parameter for estimating the radiative forcing (RF_{aci}) of Twomey effects (Gryspeerdt et al., 2023; Twomey, 1974, 1977), exhibits wide variability both in regional observations (McComiskey & Feingold, 2008) and in climate model simulations (Ghan et al., 2016; Quaas et al., 2009; Virtanen et al., 2025). Bellouin et al. (2020), in their review of bounding global aerosol radiative forcing of climate change, adopted a representative range of 0.3–0.8 for S_{aci}, following McCoy et al. (2017).

Both the classical Twomey effect (Twomey, 1974, 1977) and simulations from adiabatic parcel model (e.g., Chen et al., 2016; Reutter et al., 2009) suggest that the cloud sensitivity is modulated by cloud dynamics. At a given cloud-base updraft velocity (w), increasing N_a reduce the maximum supersaturation within the cloud, lowering the aerosol activation ratio (AR) and leading to a nonlinear response of N_C to N_a. In the aerosol-limited regime, characterized by low N_a or strong w, N_C is highly sensitive to changes in N_a, and high S_{aci} values are expected (e.g., Werner et al., 2014). In contrast, in the updraft-limited regime, where aerosols are abundant but w is weak,

Writing – review & editing: Yuan Wang

S_{aci} tends to be lower (e.g., Anil Kumar et al., 2016). Additionally, aerosol loading can actively modulate cloud dynamical conditions, further regulating in-cloud w and complicating aerosol–cloud interactions. Changes in N_a may either strengthen or weaken cloud updrafts depending on the environmental and microphysical conditions. For example, elevated aerosol loading may enhance latent heat release and invigorate convection under favorable thermodynamic conditions, leading to stronger updrafts (Abbott & Cronin, 2021; Fan et al., 2018; Sheffield et al., 2015; Yuan et al., 2011). Conversely, high aerosol loading may amplify dry-air entrainment and reduce cloud buoyancy, thereby suppressing updraft development (Dagan et al., 2015; Peters et al., 2023; Xue & Feingold, 2006). These competing effects may produce variable, often non-monotonic relationships between N_a and w in natural clouds, indicating that w may not act as an entirely independent meteorological factor during S_{aci} quantification.

Thus, estimates of S_{aci} should be constrained by w dependence. Although the importance of w is well recognized, the challenge of acquiring accurate direct measurements has led previous studies to either overlook this constraint or resort to alternative proxies, such as cloud base height, cloud thickness, liquid water content (path), and lower tropospheric stability (e.g., Harikishan et al., 2016; Jia et al., 2022; Ma et al., 2018; Saponaro et al., 2017; Wang, Jia, et al., 2024; Yang et al., 2021; Zhao et al., 2018). While these studies have shown that S_{aci} exhibits dependence on such proxy variables, the relationships are not consistent or clearly defined. Therefore, whether the dependence of S_{aci} on w follows a physically interpretable and universal pattern remains an important issue. Addressing this is key to quantifying aerosol–cloud interactions and ensuring a reliable assessment of RF_{aci}.

Compared with satellite remote sensing, in situ observations avoid issues such as the spatiotemporal mismatch between aerosols and clouds (Bellouin et al., 2020; Jia et al., 2021), offering distinct advantages for studying aerosol–cloud interactions and S_{aci}. During the South Asian summer monsoon, frequent occurrences of orographic clouds over the southern Tibetan Plateau (STP) provide a natural laboratory for studying aerosol–cloud interactions. From August to October 2023, the GACPE-STP campaign was conducted in this region (Wang, Li, et al., 2024), during which 145 cloud cases were sampled in situ (Wang et al., 2025), providing a valuable observational basis for investigating cloud sensitivity over the so-called Asian Water Tower (Liu et al., 2022).

A remaining challenge lies in estimating the cloud dynamics. Wang et al. (2025) estimated the effective water vapor supersaturation (SS) within these orographic clouds using κ-Köhler theory (Petters & Kreidenweis, 2007). Building on this, the present study estimates cloud-base w using the SS budget equation (Rogers & Yau, 1996; Twomey, 1959a, 1959b), and further investigates the dependence of S_{aci} on w, the underlying mechanisms, and implications for weighted-mean S_{aci} estimates.

2. Data and Methods

2.1. Experiment and Data

The GACPE-STP campaign was conducted in Yadong County, STP, China (27.42°N, 88.90°E; 3,136 m above sea level). A comprehensive overview of the campaign is provided by Wang, Li, et al. (2024). This study focuses on the influence of cloud dynamics on S_{aci}, using data from the following instruments. The Fog Monitor (FM, model 120; DMT Inc.) measures the cloud droplet size distributions (CDSD) in orographic clouds over a diameter range of 2–50 μm, with a sampling frequency of 1 Hz. The Cloud Condensation Nuclei Counter (CCNC, model 200; DMT Inc.) measures CCN number concentrations (N_{CCN}) under different SS levels from 0.07% to 0.7%. A full SS cycle takes approximately 1 hour. The Scanning Mobility Particle Sizer (SMPS, model 3938L50; TSI Inc.) provides measurements of the dry particle number size distribution (PNSD) across a diameter range of 18.8–685.4 nm, from which N_a is obtained by integrating the PNSD. One full scan is completed every 2 minutes. The three-dimensional scanning Doppler wind LiDAR (Wind3D 10k, LEICE Inc.) captures the 3D wind field from 103 to 7,846 m above ground level.

Cloud microphysical properties such as N_C and liquid water content (LWC) were derived by integrating the CDSD. A CDSD is identified as representing in-cloud condition when both $N_C \geq 10$ cm^{-3} and LWC ≥ 0.001 g m^{-3} are satisfied simultaneously (Deng et al., 2009; Lu et al., 2020). A cloud case is defined as a continuous period exceeding 10 min, during which more than 50% of the 1-min intervals meet the in-cloud conditions (Zhang et al., 2025). During the GACPE-STP campaign, a total of 145 orographic cloud cases were identified, comprising more than 1.15 million CDSDs. The CCN measurements under low SS conditions are

21698996, 2026, 20, Downloaded from https://agupubs.onlinelibrary.wiley.com/doi/10.1029/2026JD046935 by Jianping Huang - Lanzhou University , Wiley Online Library on [10/11/2026]. See the Terms and Conditions (https://onlinelibrary.wiley.com/terms-and-conditions) on Wiley Online Library for rules of use; OA articles are governed by the applicable Creative Commons License

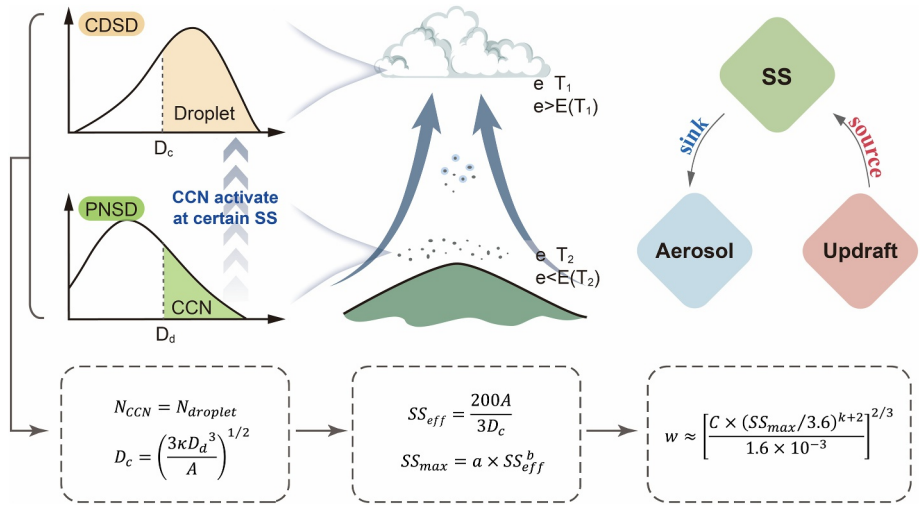


Figure 1. Schematic diagram of the calculation procedure for cloud-base updraft velocity (w).

corrected for the presence of unactivated particles using the method proposed by Wang et al. (2019) and Tao et al. (2023). The corrected $N_{CCN}(SS)$, is then fitted using a power-law function (Twomey, 1959a, 1959b) to derive the parameters C and k,

$$N_{\mathrm{CCN}} = C \times SS^{k} \tag{2}$$

where C represents the N_{CCN} at SS of 1% and k describes the slope of the fit. Equation 2 is used in the subsequent calculation of cloud dynamics in Equation 4.

2.2. Method for Estimating the Cloud Dynamics

Figure 1 presents the calculation procedure for cloud-base w. The first step involves determining the effective SS (SS_{eff}) based on simultaneous measurements of the PNSD, hygroscopicity parameter (κ), and CDSD (Wang et al., 2025). The SS_{eff} is identified as the SS at which the observed dry aerosol particles would activate to form the simultaneously observed cloud droplets. A detailed description of the SS_{eff} calculation procedure is provided in Text S1 of Supporting Information S1. The SS_{eff} derived for clouds observed during the GACPE-STP campaign, as well as the verification of the reliability, are presented in Wang et al. (2025).

Then, the maximum SS in each cloud parcel profile (SS_{max}) is calculated using an adiabatic parcel model. Field observations during the campaign indicate that the STP orographic clouds were generally shallow, with the CDSD observed during GACPE-STP estimated to lie within ~200 m above the cloud base, based on the relative location of the observation site within the clouds. Photographs of the shallow orographic clouds and the observation site are shown in Figure 2. The approximate vertical offset between cloud base and the mountaintop site (within ~200 m above cloud base) is empirically estimated from field experience. The parcel model is described in detail in Text S2 of Supporting Information S1. In the simulations, the N_a varies from 100 to 12,800 cm^{-3} and w ranges from 0.1 to 12.8 m s^{-1}, both increasing by successive doubling. The initial relative humidity is set to 80% and 90%. A total of 128 parcel simulations is conducted. Based on these, the relationship between SS_{max} and the SS_{eff} within 200 m above cloud base under different initial conditions is derived (Figure S1 in Supporting Information S1, and their fitting is given by

$$SS_{\mathrm{max}} = 1.49 SS_{\mathrm{eff}}^{\,0.65} \tag{3}$$

with R^2 of 0.89. Accordingly, SS_{max} can then be obtained. It is worth noting that assuming the observations are located within different height ranges above cloud base may slightly alter the fitting coefficients in Equation 3 (Figure S1 in Supporting Information S1), thereby affecting the values of SS_{max} and the subsequently derived w. However, this does not change the relative variation or trend of w (Figure S2 in Supporting Information S1).

21698996, 2026, 20, Downloaded from https://agupubs.onlinelibrary.wiley.com/doi/10.1029/2026JD046935 by Jianping Huang - Lanzhou University , Wiley Online Library on [10/11/2026]. See the Terms and Conditions (https://onlinelibrary.wiley.com/terms-and-conditions) on Wiley Online Library for rules of use; OA articles are governed by the applicable Creative Commons License



Figure 2. Photographs of the observation site and the STP shallow orographic clouds.

Finally, as cloud dynamics and water vapor condensation onto aerosols and droplets serve as the source and sink terms of SS_{max}, respectively (Korolev & Mazin, 2003), the cloud-base w can be estimated using the derived SS_{max} and the power-law activation parameters C and k in Equation 2 (Rogers & Yau, 1996; Twomey, 1959a, 1959b):

$$w \approx \left[\frac{C \times (SS_{max}/3.6)^{k+2}}{1.6 \times 10^{-3}}\right]^{2/3} \quad (4)$$

In this study, only the initial hour of each cloud case was analyzed, as longer durations tend to involve non-adiabatic effects (e.g., advection and sedimentation) that reduces the accuracy of SS and w estimations. The effect of entrainment is also neglected, which may lead to underestimation of both SS and w through its reduction of N_C (Lu et al., 2011, 2023; Tölle & Krueger, 2014). The retrieved cloud-base w is shown in Figure 3a. Its probability distribution exhibits an approximately normal shape, with 98.1% of values falling within the range of 0.1–10 m s^{-1}. For validation against Doppler-LiDAR observations, both retrieved cloud-base w and LiDAR-derived w are aggregated to cloud-event-averaged values. Since the observation site resides above the orographic cloud base, the lowest available LiDAR measurement level at 103 m above ground is the closest proxy for near-cloud-base conditions and is therefore used for comparison. As illustrated in Figure 3b, the retrieved cloud-base w is significantly correlated with LiDAR-derived w ($r = 0.84$, $p < 0.01$). This significant correlation supports the reliability of the cloud-base w estimates. Despite this favorable agreement, we do not directly use LiDAR-derived w to characterize cloud dynamical conditions in this study. The dynamic driver governing cloud activation corresponds specifically to cloud-base w, yet the LiDAR-derived w represents the value at a height

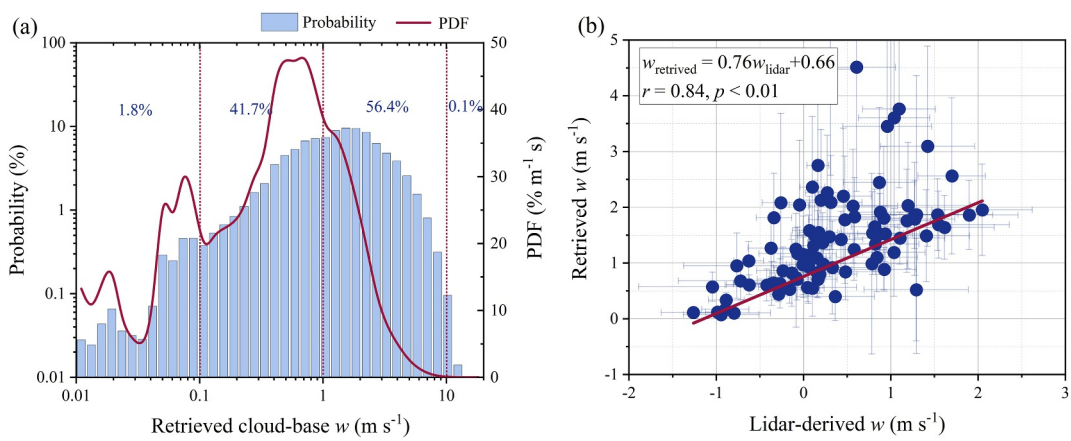


Figure 3. (a) Probability density function (PDF) of the retrieved cloud-base updraft velocity (w), together with the probability distribution across different w ranges. (b) Comparison of cloud-event-averaged w derived from Doppler LiDAR versus retrieved cloud-base w from this study. Error bars denote one standard deviation.

21698996, 2026, 20, Downloaded from https://agupubs.onlinelibrary.wiley.com/doi/10.1029/2026JD046935 by Jianping Huang - Lanzhou University , Wiley Online Library on [10/11/2026]. See the Terms and Conditions (https://onlinelibrary.wiley.com/terms-and-conditions) on Wiley Online Library for rules of use; OA articles are governed by the applicable Creative Commons License

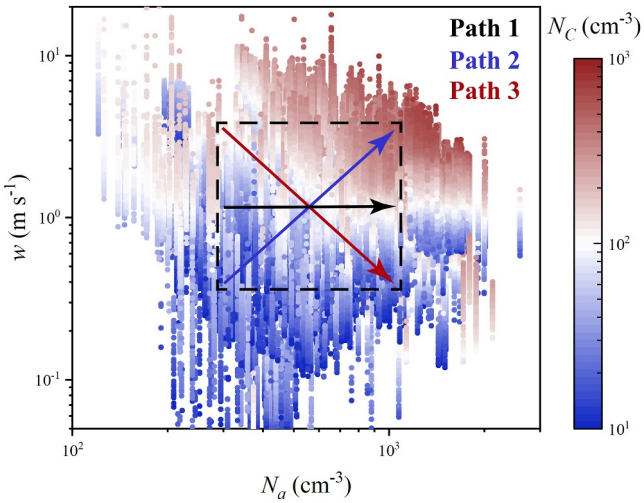


Figure 4. Joint dependence of N_C on N_a and w. Three arrows indicate different pathways of N_C variation in response to N_a changes.

103 m above the observation site. This discrepancy arises because the bases of orographic clouds were persistently lower than the observation site altitude during FM measurements of CDSDs, meaning the observation site was situated within the cloud interior.

3. Results

3.1. Cloud Sensitivity Constrained by Cloud Dynamics

Figure 4 presents in situ observations of the joint distribution of N_C with N_a and w. When either w or N_a is held constant, N_C increases with the other variable, indicating that N_C is modulated by the combined influence of N_a and w. The corresponding joint distributions of SS and AR with N_a and w are provided in Figure S3 of Supporting Information S1. Three arrows in Figure 4 illustrate idealized N_a enhancement pathways under different w change scenarios, highlighting how N_C responds to increases in N_a when w is fixed, increases, or decreases. Studies of the Twomey effect typically assume constant w, attributing N_C variations solely to changes in N_a. However, in reality, w is not constant but varies among clouds. If N_a increases alongside an increase in w (blue path in Figure 4), the sensitivity of N_C to N_a is amplified, potentially leading to a S_{aci} greater than 1. Conversely, if N_a increases while w decreases (red path), cloud sensitivity is suppressed, and negative S_{aci} values may occur, a phenomenon referred to as the anti-Twomey effect (e.g., Jose et al., 2020; Yuan et al., 2008). Physically, negative S_{aci} reflects a negative covariance between aerosol loading and cloud-base updraft: higher aerosol concentrations tend to coincide with weaker updrafts. This covariation counteracts the expected aerosol-driven increase in cloud-droplet number and yields the suppressed or even negative sensitivity. In natural atmospheric conditions, clouds may exhibit more complex responses, where w may be uncorrelated with N_a or vary non-monotonically with N_a. Therefore, ignoring the variation of w when assessing the sensitivity of N_C to N_a introduces biases due to the intrinsic dependence of N_C on w, leading to inaccurate quantification of S_{aci}.

Figure 5 presents the relationships between N_C and N_a under conditions with and without w constraints. In the log–log coordinate system, the slope of the linear regression between N_C and N_a represents the S_{aci}. Figure 5a shows the S_{aci} without constraining w, obtained by fitting the relationship between case-averaged N_C and N_a, resulting in a S_{aci} of 0.836. Calculating S_{aci} using the relationship between case-averaged cloud and aerosol properties without constraining w, or by assuming uniform w across clouds, has been widely adopted in previous aerosol–cloud interaction studies (e.g., de Graaf et al., 2023; Jia et al., 2019; Ma et al., 2010; Virtanen et al., 2025). In Figure 5b, w values ranging from 0.1 to 10 m s^{-1} are divided into 12 logarithmically spaced bins. Cloud sensitivity is then evaluated within each bin to constrain w and examine how S_{aci} varies with w. Cases with w less than 0.1 or larger than 10 m s^{-1} are excluded from the bin-wise analysis due to insufficient sample sizes. When w is low (first 5 bins, $w < 0.68$ m s^{-1}), N_C shows little sensitivity to increases in N_a, with S_{aci} approaching 0, indicating that additional aerosols do not activate into more cloud droplets. In contrast, when w is high (last 5 bins, $w > 1.47$ m s^{-1}), N_C becomes highly sensitive to N_a, with S_{aci} approaching 1. As w increases from 0.68 to 1.47 m s^{-1}, S_{aci} rapidly transitions from 0 to 1. Therefore, as shown in Figure 6a, cloud sensitivity exhibits a sigmoid-shaped dependence on w, initially near 0, then rising sharply, and eventually plateauing near 1. The fitted S_{aci}, sample size, and corresponding 95% confidence intervals for each bin are provided in Table S1 of Supporting Information S1. In low-w bins confidence intervals are broad and mostly contain zero, while for high-w bins confidence intervals move away from zero but frequently include the theoretical Twomey limit of 1. The sigmoid fitting result is shown in Figure 8a,

$$S_{\mathrm{aci}} = \frac{1.01}{1 + \exp(-5.67(w - 1.11))} \tag{5}$$

with an R^2 of 0.97. The critical w, defined as the w value corresponding to half of the S_{aci}, is 1.11 m s^{-1}, which determines the inflection point of the sigmoid curve. Additionally, we examined different bin numbers for w

21698996, 2026, 20, Downloaded from https://agupubs.onlinelibrary.wiley.com/doi/10.1029/2026JD046935 by Jianping Huang - Lanzhou University , Wiley Online Library on [10/11/2026]. See the Terms and Conditions (https://onlinelibrary.wiley.com/terms-and-conditions) on Wiley Online Library for rules of use; OA articles are governed by the applicable Creative Commons License

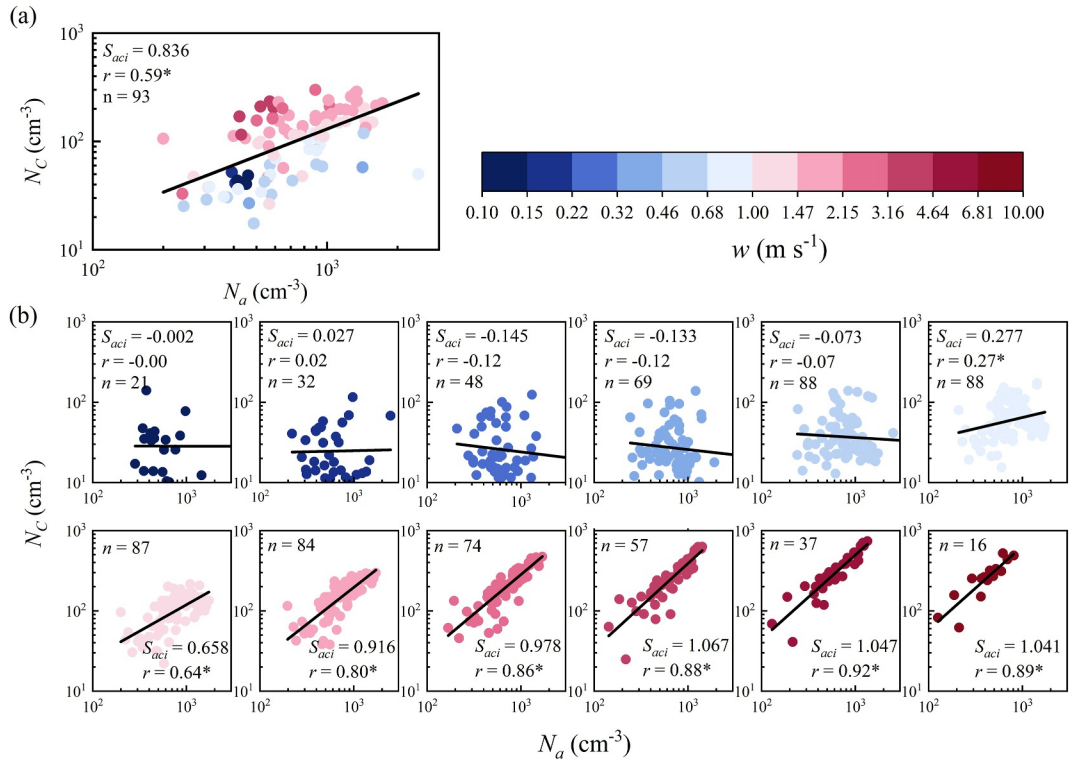


Figure 5. Relationship between N_C and N_a under two conditions: (a) without constraining w, and (b) with w constrained by dividing it into 12 bins. Black lines represent linear fits of N_C versus N_a in log–log space, where S_{aci} denotes the fitting slope, representing the sensitivity of N_C to N_a. Asterisks indicate statistically significant correlations at the 0.05 significance level. The sample size (n) for each w bin is annotated within each sub-panel.

(from 5 to 12) and found that the sigmoid-shaped dependence of S_{aci} on w remains consistent, indicating that the result is not sensitive to the number of bins (Figure S4 in Supporting Information S1).

3.2. Underlying Mechanisms

To explain the sigmoid-shaped dependence of S_{aci} on w, we consider both cloud microphysics and mathematical perspectives. N_C equals the product of AR and N_a, so S_{aci} can be reformulated as:

$$S_{aci} = 1 + \frac{d\ln AR}{d\ln N_a} \tag{6}$$

where AR primarily depends on SS. w and N_a serve as the source and sink terms of SS, respectively. When w is fixed, an increase in N_a leads to a decrease in SS (Figure S3a in Supporting Information S1). Within each w bin, the sensitivity of AR to changes in N_a is shown in Figure 7. Under low w conditions, SS remains generally low and AR is highly sensitive to SS changes. Consequently, increases in N_a substantially reduce SS, leading to a pronounced decrease in AR. The sensitivity of AR to N_a ($d\ln AR/d\ln N_a$) is approximately -1, which yields a S_{aci} close to 0, characteristic of the updraft-limited regime. Under high w conditions, SS is generally high, and AR becomes insensitive to SS changes. Although increases in N_a still reduces SS, AR remains nearly constant, with the sensitivity of AR to N_a close to 0. This results in a S_{aci} close to 1, characteristic of the aerosol-limited regime. Between these two regimes lies a transition regime, where the sensitivity of AR to N_a ranges between -1 and 0, causing S_{aci} to gradually increase from 0 to 1. Therefore, the sigmoid-shape dependence of AR sensitivity to N_a on w underlies the observed sigmoid relationship between S_{aci} on w, as shown in Figure 6a.

From a cloud microphysics perspective, it is necessary to further explain why AR is more sensitive to SS changes under low-SS conditions but becomes less sensitive at high SS. According to the κ-Köhler equation (Petters & Kreidenweis, 2007), assuming constant hygroscopicity parameter (κ), an increase in SS leads to a decrease in dry

21698996, 2026, 20, Downloaded from https://agupubs.onlinelibrary.wiley.com/doi/10.1029/2026JD046935 by Jianping Huang - Lanzhou University , Wiley Online Library on [10/11/2026]. See the Terms and Conditions (https://onlinelibrary.wiley.com/terms-and-conditions) on Wiley Online Library for rules of use; OA articles are governed by the applicable Creative Commons License

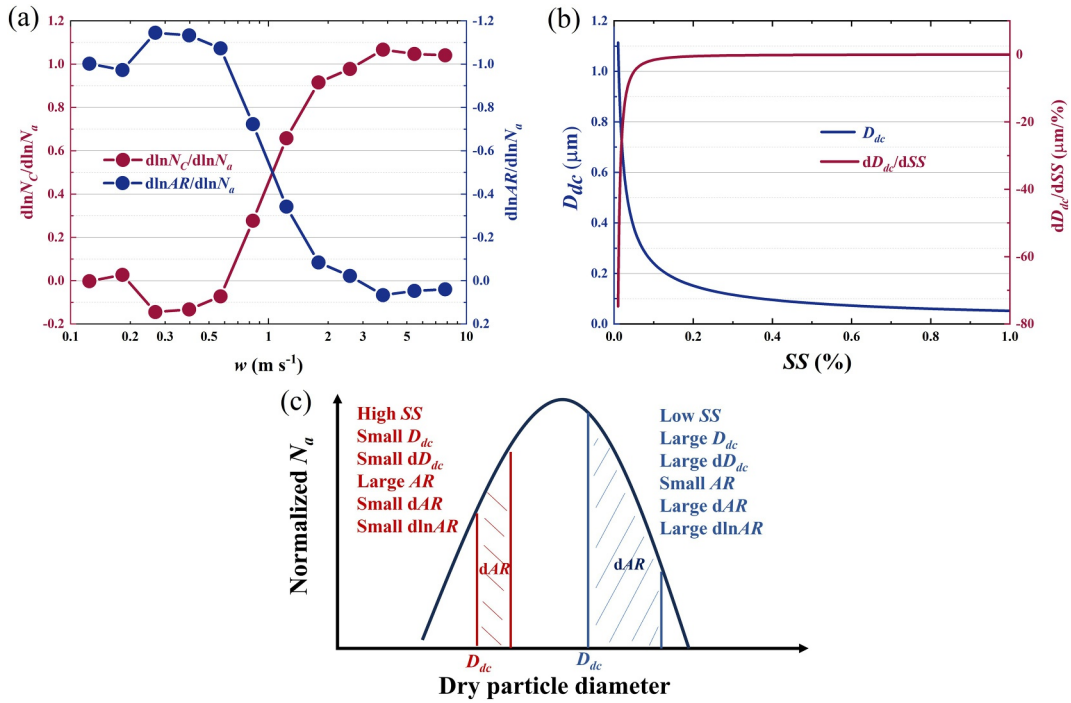


Figure 6. (a) Dependence of dlnN_C/dlnN_a and dlnAR/dlnN_a on w; (b) Variation of dry aerosol critical activation diameter (D_{dc}) with supersaturation (SS), and the corresponding differential (dD_{dc}/dSS) as a function of SS from the κ-Köhler equation; (c) Schematic comparisons of D_{dc}, dD_{dc}, AR, dAR, and dlnAR, under high and low SS conditions. Black curve represents the normalized dry PNSD.

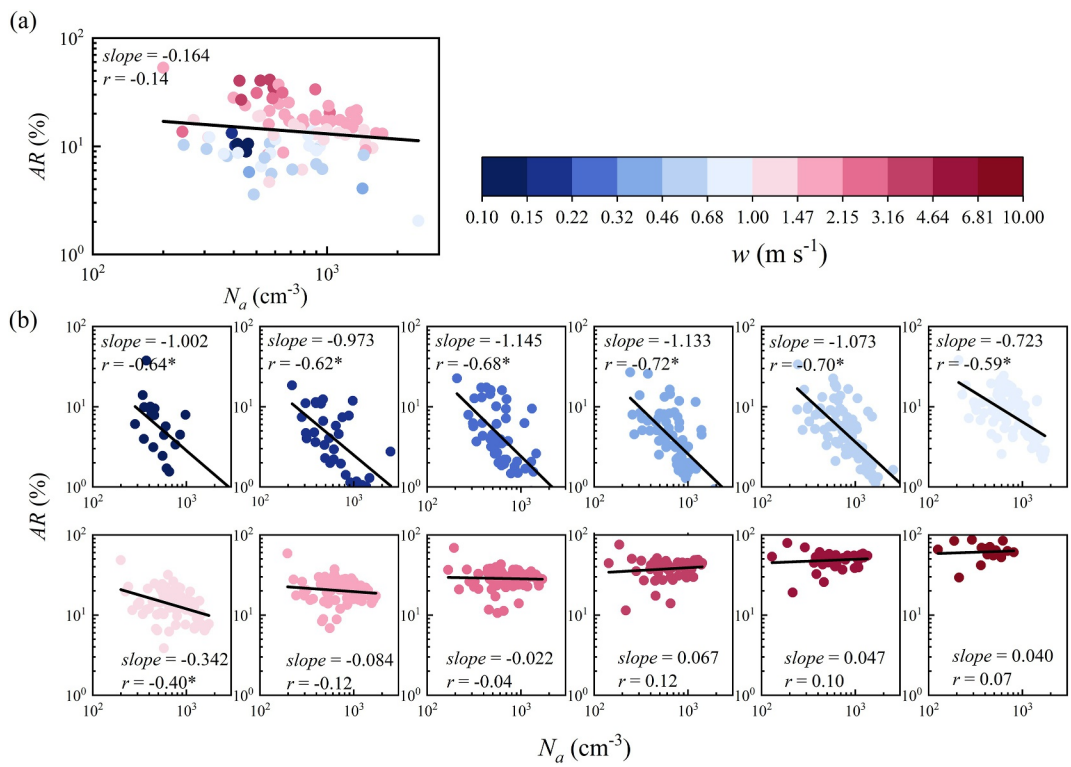


Figure 7. Same as Figure 5 but for the relationships between aerosol activation ratio (AR) and aerosol number concentration (N_a).

21698996, 2026, 20, Downloaded from https://agupubs.onlinelibrary.wiley.com/doi/10.1029/2026JD046935 by Jianping Huang - Lanzhou University , Wiley Online Library on [10/11/2026]. See the Terms and Conditions (https://onlinelibrary.wiley.com/terms-and-conditions) on Wiley Online Library for rules of use; OA articles are governed by the applicable Creative Commons License

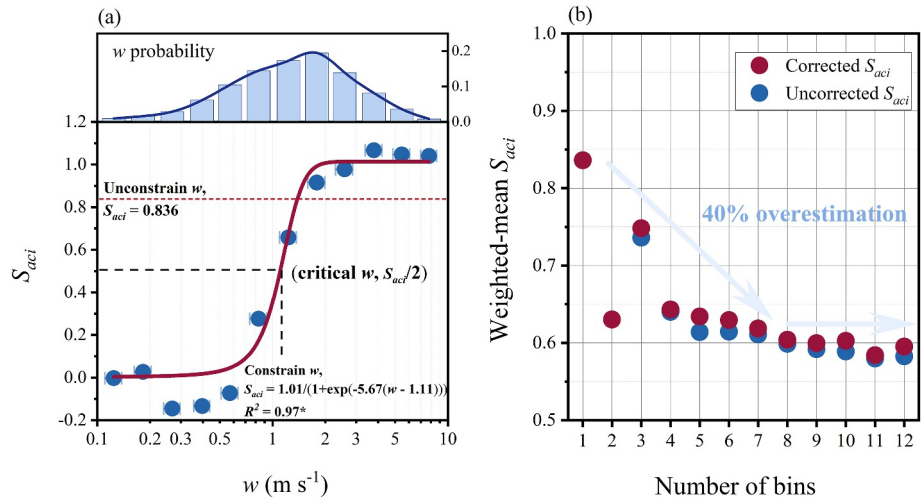


Figure 8. (a) Dependence of S_{aci} on w, and w probability distribution; (b) variation of the weighted-mean S_{aci} as a function of the number of w bins. Red curve indicates the Sigmoid fit.

aerosol critical activation diameter (D_{dc}). The reduction in D_{dc} per unit increase in SS (dD_{dc}/dSS) is much larger at low SS than at high SS, as shown in Figure 6b. Consequently, at low SS, a unit increase in SS results in a greater increase in AR, whereas the opposite occurs at high SS, as illustrated in Figure 6c. Therefore, AR is more sensitive to changes in SS at low SS but less sensitive at high SS.

Additionally, from a mathematical perspective, the definition of $d\ln AR$ represents the relative change in AR, which equals the absolute change (dAR) divided by AR. Under high-w (and thus high-SS) conditions, both a smaller dAR (Figure 6c) and a larger AR value result in $d\ln AR$ approaching 0, leading to S_{aci} approaching 1. Conversely, under low-w (low-SS) conditions, dAR is larger while AR is smaller, causing $d\ln AR$ to approach -1 and S_{aci} to approach 0. These combined effects give rise to the observed sigmoid dependence of S_{aci} on w.

3.3. Overestimation of Cloud Sensitivity

Accurate calculation of S_{aci} is crucial for estimating RF_{aci}, as biases in the estimation of S_{aci} directly translate into errors in the assessment of the RF_{aci} (Bellouin et al., 2020). Without constraining w, the S_{aci} is 0.836 (Figure 5a). When w is constrained, S_{aci} varies with w and exhibits a sigmoid-shaped distribution (Figure 8a). Therefore, the regional mean S_{aci} should be calculated as a weighted average across different w bins, yielding a weighted-mean S_{aci} value of 0.583. After bounding the S_{aci} values within each bin (setting $S_{aci} < 0$ to 0 and >1 to 1), the corrected weighted-mean S_{aci} becomes 0.595. Consequently, ignoring the w constraint leads to a 40% overestimation of S_{aci}, which in turn could result in a comparable (~40%) overestimation of RF_{aci} for STP orographic clouds, assuming other factors (e.g., aerosol optical thickness, cloud albedo sensitivity to N_C, and effective cloud fraction) remain unaffected.

Whether S_{aci} values are corrected to fall within 0–one in each bin has only a minor impact on the weighted-mean S_{aci}, as shown in Figure 8b. For example, when the data are divided into 12 bins, the weighted-mean S_{aci} differs by only 2% between the corrected and uncorrected cases. Furthermore, the weighted-mean S_{aci} tends to converge with increasing numbers of w bins. When the number of bins is fewer than eight, the weighted-mean S_{aci} decreases as the number of bins increases. When the number of bins exceeds eight, further increases have little impact on the weighted-mean S_{aci}.

Additionally, we assess the impact of different assumptions regarding the distance above cloud base on the weighted-mean S_{aci}, as shown in Figure 9. The results show that variations in the assumed height above cloud base (HACB) do not affect the main conclusions of this study. Specifically, S_{aci} still exhibits a sigmoid dependence on w, and ignoring the w constraint still leads to an overestimation of weighted-mean S_{aci}. However, these assumptions do influence the calculated SS_{max} and w values (Figure S2 in Supporting Information S1), which in turn affect the critical w and the extent of weighted-mean S_{aci} overestimation. Across tested HACB thresholds of 50–200 m, the critical w varies between 0.48 and 1.11 m s^{-1} and the weighted-mean S_{aci} overestimation spans

21698996, 2026, 20, Downloaded from https://agupubs.onlinelibrary.wiley.com/doi/10.1029/2026JD046935 by Jianping Huang - Lanzhou University , Wiley Online Library on [10/11/2026]. See the Terms and Conditions (https://onlinelibrary.wiley.com/terms-and-conditions) on Wiley Online Library for rules of use; OA articles are governed by the applicable Creative Commons License

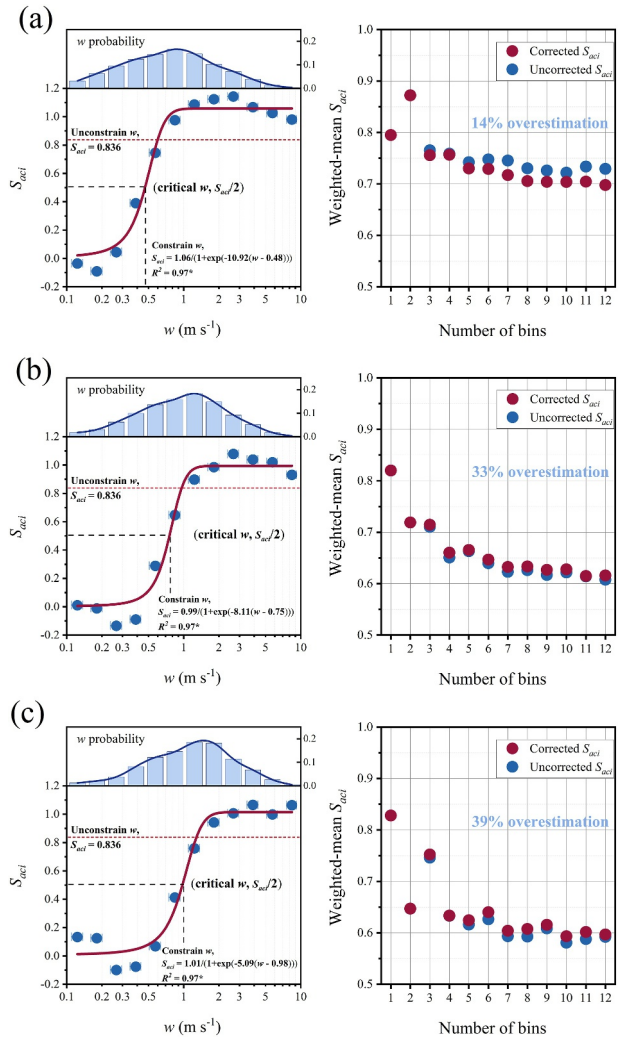


Figure 9. Same as Figure 8, but assuming within different heights above cloud base (HACB) to retrieve cloud-base updraft velocity. The selected HACB values are: (a) 50 m, (b) 100 m, and (c) 150 m.

14%–40%. For instance, when the assumed HACB is changed from 200 to 100 m, the critical w decreases from 1.11 to 0.75 m s^{-1}, and the overestimation of S_{aci} is reduced from 40% to 33%.

4. Conclusions and Discussions

This study demonstrates that the sensitivity of N_C to N_a is strongly modulated by cloud dynamics, and therefore S_{aci} estimates must appropriately account for dynamical dependence on w. Using in situ measurements from the GACPE-STP campaign and adiabatic cloud parcel model simulations, we estimate w by explicitly resolving the source and sink terms of SS, enabling an assessment of how w-dependence shapes S_{aci} estimates.

Results show that when w is binned, S_{aci} increases with w and exhibits a sigmoid-shaped distribution. The corrected regional mean S_{aci}, calculated as the w-weighted average, is 0.595, lower than the unconstrained value of 0.836. For STP orographic clouds, our analysis yields a 14%–40% overestimation of S_{aci}, which suggests a comparable bias in RF_{aci} under the assumption that other factors are unaffected by w constraints. This quantitative offset is specific to the present study region, cloud regime and methodological setup. Terrain slope and altitude can further modulate the magnitude of this bias. Steep high-elevation mountain slopes over the STP produce a broad range of terrain-driven w, amplifying the dynamical modulation on S_{aci}; by contrast, gentler or lower-elevation mountain terrain would generate narrower and weaker w distributions, which may yield different bias magnitudes. For convective clouds, dynamical overestimation of S_{aci} may occur in weak-updraft regions but is suppressed as S_{aci} saturates under strong lifting. Ice-phase microphysics, entrainment and storm evolution further complicate aerosol-cloud interactions, such that the ~40% bias cannot be directly extrapolated to convective clouds and deserves dedicated investigations. Nevertheless, neglecting dynamical constraints does not necessarily lead to an overestimation of S_{aci}, as the effect can be region dependent. For instance, in a well-mixed and turbulent marine boundary layer with a w distribution resembling the upper end of Figure 8a, S_{aci} may instead be underestimated or remain largely unchanged.

The emergence of the sigmoid pattern arises from Köhler activation theory and S_{aci} mathematical definition. It is thus theoretically expected to hold across diverse cloud regimes, though direct observational validation (e.g., in marine stratocumulus or deep convection) remains to be tested. Additionally, in polluted environments, higher w is required to transition out of the updraft-limited regime, potentially obscuring the full sigmoid pattern. Moreover, regional variability in the critical w arises from its dependence on SS, which scales with w/N_a (Figure S5 in Supporting Information S1). To account for variability in measured PNSD size range, we propose an empirical relationship linking the critical w to the Twomey power-law coefficient C (Equation 2), based on observations of STP orographic clouds during the GACPE-STP campaign:

$$\text{critical } w = 1.25 \times 10^{-3} \times C \tag{7}$$

where C is in cm^{-3} and critical w is in m s^{-1}. Finally, the distribution of w across different cloud regimes (e.g., continental vs. marine, stratiform vs. cumuliform) can lead to variations in the weighted-average S_{aci} and thus impact RF_{aci} estimates.

One important caveat is potential circularity within our observational-diagnostic workflow. Both S_{aci} and w are derived from the same set of observations, including dry PNSD, CCN, and CDSD, while w retrieval further employs Köhler-theory-based parameterizations for supersaturation and aerosol activation. S_{aci} is diagnosed purely from observed aerosol and cloud droplet number concentrations without Köhler-based parameterizations.

21698996, 2026, 20, Downloaded from https://agupubs.onlinelibrary.wiley.com/doi/10.1029/2026JD046935 by Jianping Huang - Lanzhou University , Wiley Online Library on [10/11/2026]. See the Terms and Conditions (https://onlinelibrary.wiley.com/terms-and-conditions) on Wiley Online Library for rules of use; OA articles are governed by the applicable Creative Commons License

21698996, 2026, 20, Downloaded from https://agupubs.onlinelibrary.wiley.com/doi/10.1029/2026JD046935 by Jianping Huang - Lanzhou University , Wiley Online Library on [10/11/2026]. See the Terms and Conditions (https://onlinelibrary.wiley.com/terms-and-conditions) on Wiley Online Library for rules of use; OA articles are governed by the applicable Creative Commons License

Collocated wind-radar observations show a positive correlation with retrieved w, supporting its variability. Nevertheless, shared observational inputs and Köhler-related retrieval assumptions may modulate the magnitude, inflection point, and detailed shape of the sigmoid S_{aci}-w covariation. Though this sigmoid feature is not hard-coded into our retrieval, complete isolation from such coupling effects cannot be achieved with current data and should be considered when interpreting our results.

From an observational perspective, accurately constraining S_{aci} remains critical for robust assessments of aerosol–cloud interactions and model evaluations. This study presents a novel framework for estimating cloud sensitivity by explicitly incorporating dynamical constraints and demonstrates that cloud sensitivity exhibits a sigmoid dependence on cloud dynamics. Importantly, a mechanistic explanation is provided, suggesting that this sigmoid pattern may be broadly applicable across different cloud regimes. Nevertheless, its broad applicability and implications still require further validation through additional observations.

Conflict of Interest

The authors declare no conflicts of interest relevant to this study.

Availability Statement

Data used in this study are available at https://doi.org/10.6084/m9.figshare.28675295.v5, corresponding to the dataset described in Fang and Wang (2025).

Acknowledgments
This research is supported by the NSFC Regional Innovation and Development Joint Fund (U24A20604), the NSFC Innovative Research Group Project (42421001), the National Natural Science Foundation of China (42575074), the Second Tibetan Plateau Scientific Expedition and Research Program (2019QZKK0602), the Fundamental Research Funds for the Central Universities (lzujbky-2026-jdzx07), and the Supercomputing Center of Lanzhou University.

References

Abbott, T. H., & Cronin, T. W. (2021). Aerosol invigoration of atmospheric convection through increases in humidity. *Science*, *371*(6524), 83–85. https://doi.org/10.1126/science.abc5181

Anil Kumar, V., Pandithurai, G., Leena, P. P., Dani, K. K., Murugavel, P., Sonbawne, S. M., et al. (2016). Investigation of aerosol indirect effects on monsoon clouds using ground-based measurements over a high-altitude site in Western Ghats. *Atmospheric Chemistry and Physics*, *16*(13), 8423–8430. https://doi.org/10.5194/acp-16-8423-2016

Bellouin, N., Quaas, J., Gryspeerdt, E., Kinne, S., Stier, P., Watson-Parris, D., et al. (2020). Bounding global aerosol radiative forcing of climate change. *Reviews of Geophysics*, *58*(1), e2019RG000660. https://doi.org/10.1029/2019RG000660

Chen, J., Liu, Y., Zhang, M., & Pen, Y. (2016). New understanding and quantification of the regime dependence of aerosol-cloud interaction for studying aerosol indirect effects. *Geophysical Research Letters*, *43*(4), 1780–1787. https://doi.org/10.1002/2016GL067683

Dagan, G., Koren, I., & Altaratz, O. (2015). Competition between core and periphery-based processes in warm convective clouds–from invigoration to suppression. *Atmospheric Chemistry and Physics*, *15*(5), 2749–2760. https://doi.org/10.5194/acp-15-2749-2015

de Graaf, M., Sarna, K., Brown, J., Tenner, E. V., Schenkels, M., & Donovan, D. P. (2023). Aerosol first indirect effect of African smoke at the cloud base of marine cumulus clouds over Ascension Island, southern Atlantic Ocean. *Atmospheric Chemistry and Physics*, *23*(9), 5373–5391. https://doi.org/10.5194/acp-23-5373-2023

Deng, Z., Zhao, C., Zhang, Q., Huang, M., & Ma, X. (2009). Statistical analysis of microphysical properties and the parameterization of effective radius of warm clouds in Beijing area. *Atmospheric Research*, *93*(4), 888–896. https://doi.org/10.1016/j.atmosres.2009.04.011

Fan, J., Rosenfeld, D., Zhang, Y., Giangrande, S. E., Li, Z., Machado, L. A. T., et al. (2018). Substantial convection and precipitation enhancements by ultrafine aerosol particles. *Science*, *359*(6374), 411–418. https://doi.org/10.1126/science.aan8461

Fang, F., & Wang, Y. (2025). In-Situ observations of orographic clouds over the Southern Tibetan Plateau [Dataset]. *Figshare*. https://doi.org/10.6084/m9.figshare.28675295.v5

Ghan, S., Wang, M., Zhang, S., Ferrachat, S., Gettelman, A., Griesfeller, J., et al. (2016). Challenges in constraining anthropogenic aerosol effects on cloud radiative forcing using present-day spatiotemporal variability. *Proceedings of the National Academy of Sciences of the United States of America*, *113*(21), 5804–5811. https://doi.org/10.1073/pnas.1514036113

Gryspeerdt, E., Povey, A. C., Grainger, R. G., Hasekamp, O., Hsu, N. C., Mulcahy, J. P., et al. (2023). Uncertainty in aerosol–cloud radiative forcing is driven by clean conditions. *Atmospheric Chemistry and Physics*, *23*(7), 4115–4122. https://doi.org/10.5194/acp-23-4115-2023

Harikishan, G., Padmakumari, B., Maheskumar, R. S., Pandithurai, G., & Min, Q. L. (2016). Aerosol indirect effects from ground-based retrievals over the rain shadow region in Indian subcontinent. *Journal of Geophysical Research: Atmospheres*, *121*(5), 2369–2382. https://doi.org/10.1002/2015JD024577

IPCC. (2021). In V. Masson-Delmotte, P. Zhai, A. Pirani, S. L. Connors, C. Péan, et al. (Eds.), *Climate Change 2021: The physical science basis. Contribution of working group I to the sixth assessment report of the intergovernmental panel on climate change* (p. 959). Cambridge University Press. https://doi.org/10.1017/9781009157896

Jia, H., Ma, X., Yu, F., Liu, Y., & Yin, Y. (2019). Distinct impacts of increased aerosols on cloud droplet number concentration of Stratus/Stratocumulus and cumulus. *Geophysical Research Letters*, *46*(22), 13517–13525. https://doi.org/10.1029/2019GL085081

Jia, H., Ma, X., Yu, F., & Quaas, J. (2021). Significant underestimation of radiative forcing by aerosol–cloud interactions derived from satellite-based methods. *Nature Communications*, *12*(1), 3649. https://doi.org/10.1038/s41467-021-23888-1

Jia, H., Quaas, J., Gryspeerdt, E., Böhm, C., & Sourdeval, O. (2022). Addressing the difficulties in quantifying droplet number response to aerosol from satellite observations. *Atmospheric Chemistry and Physics*, *22*(11), 7353–7372. https://doi.org/10.5194/acp-22-7353-2022

Jose, S., Nair, V. S., & Babu, S. S. (2020). Anthropogenic emissions from South Asia reverses the aerosol indirect effect over the northern Indian Ocean. *Scientific Reports*, *10*(1), 18360. https://doi.org/10.1038/s41598-020-74897-x

Korolev, A. V., & Mazin, I. P. (2003). Supersaturation of water vapor in clouds. *Journal of the Atmospheric Sciences*, *60*(24), 2957–2974. https://doi.org/10.1175/1520-0469(2003)060<2957:SOWVIC>2.0.CO;2

Liu, Y., Huang, J., Wang, T., Li, J., Yan, H., & He, Y. (2022). Aerosol-cloud interactions over the Tibetan Plateau: An overview. *Earth-Science Reviews*, *234*, 104216. https://doi.org/10.1016/j.earscirev.2022.104216

Lu, C., Liu, Y., & Niu, S. (2011). Examination of turbulent entrainment-mixing mechanisms using a combined approach. *Journal of Geophysical Research*, *116*(D20), D20207. https://doi.org/10.1029/2011JD015944

Lu, C., Liu, Y., Yum, S. S., Chen, J., Zhu, L., Gao, S., et al. (2020). Reconciling contrasting relationships between relative dispersion and volume-mean radius of Cloud droplet size distributions. *Journal of Geophysical Research: Atmospheres*, *125*(9), e2019JD031868. https://doi.org/10.1029/2019JD031868

Lu, C., Zhu, L., Liu, Y., Mei, F., Fast, J. D., Pekour, M. S., et al. (2023). Observational study of relationships between entrainment rate, homogeneity of mixing, and cloud droplet relative dispersion. *Atmospheric Research*, *293*, 106900. https://doi.org/10.1016/j.atmosres.2023.106900

Ma, J., Chen, Y., Wang, W., Yan, P., Liu, H., Yang, S., et al. (2010). Strong air pollution causes widespread haze-clouds over China. *Journal of Geophysical Research*, *115*(D18), 2009JD013065. https://doi.org/10.1029/2009JD013065

Ma, X., Jia, H., Yu, F., & Quaas, J. (2018). Opposite aerosol index-cloud droplet effective radius correlations over major industrial regions and their adjacent Oceans. *Geophysical Research Letters*, *45*(11), 5771–5778. https://doi.org/10.1029/2018GL077562

McComiskey, A., & Feingold, G. (2008). Quantifying error in the radiative forcing of the first aerosol indirect effect. *Geophysical Research Letters*, *35*(2). https://doi.org/10.1029/2007GL032667

McCoy, D. T., Bender, F. a.-M., Mohrmann, J. K. C., Hartmann, D. L., Wood, R., & Grosvenor, D. P. (2017). The global aerosol-cloud first indirect effect estimated using MODIS, MERRA, and AeroCom. *Journal of Geophysical Research: Atmospheres*, *122*(3), 1779–1796. https://doi.org/10.1002/2016JD026141

Peters, J. M., Lebo, Z. J., Chavas, D. R., & Su, C.-Y. (2023). Entrainment makes pollution more likely to weaken deep convective updrafts than invigorate them. *Geophysical Research Letters*, *50*(12), e2023GL103314. https://doi.org/10.1029/2023GL103314

Petters, M. D., & Kreidenweis, S. M. (2007). A single parameter representation of hygroscopic growth and cloud condensation nucleus activity. *Atmospheric Chemistry and Physics*, *7*(8), 1961–1971. https://doi.org/10.5194/acp-7-1961-2007

Quaas, J., Ming, Y., Menon, S., Takemura, T., Wang, M., Penner, J. E., et al. (2009). Aerosol indirect effects—General circulation model intercomparison and evaluation with satellite data. *Atmospheric Chemistry and Physics*, *9*(22), 8697–8717. https://doi.org/10.5194/acp-9-8697-2009

Reutter, P., Su, H., Trentmann, J., Simmel, M., Rose, D., Gunthe, S. S., et al. (2009). Aerosol- and updraft-limited regimes of cloud droplet formation: Influence of particle number, size and hygroscopicity on the activation of cloud condensation nuclei (CCN). *Atmospheric Chemistry and Physics*, *9*(18), 7067–7080. https://doi.org/10.5194/acp-9-7067-2009

Rogers, R. R., & Yau, M. K. (1996). *A short course in cloud physics* (3rd ed.). Butterworth-Heinemann.

Saponaro, G., Kolmonen, P., Sogacheva, L., Rodriguez, E., Virtanen, T., & de Leeuw, G. (2017). Estimates of the aerosol indirect effect over the Baltic Sea region derived from 12 years of MODIS observations. *Atmospheric Chemistry and Physics*, *17*(4), 3133–3143. https://doi.org/10.5194/acp-17-3133-2017

Sheffield, A. M., Saleeby, S. M., & van den Heever, S. C. (2015). Aerosol-induced mechanisms for cumulus congestus growth. *Journal of Geophysical Research: Atmospheres*, *120*(17), 8941–8952. https://doi.org/10.1002/2015JD023743

Tao, J., Kuang, Y., Luo, B., Liu, L., Xu, H., Ma, N., et al. (2023). Kinetic limitations affect cloud condensation nuclei activity measurements under low supersaturation. *Geophysical Research Letters*, *50*(4), e2022GL101603. https://doi.org/10.1029/2022GL101603

Tölle, M. H., & Krueger, S. K. (2014). Effects of entrainment and mixing on droplet size distributions in warm cumulus clouds. *Journal of Advances in Modeling Earth Systems*, *6*(2), 281–299. https://doi.org/10.1002/2012MS000209

Twomey, S. (1959a). The nuclei of natural cloud formation part I: The chemical diffusion method and its application to atmospheric nuclei. *Geofisica Pura e Applicata*, *43*(1), 227–242. https://doi.org/10.1007/BF01993559

Twomey, S. (1959b). The nuclei of natural cloud formation part II: The supersaturation in natural clouds and the variation of cloud droplet concentration. *Geofisica Pura e Applicata*, *43*(1), 243–249. https://doi.org/10.1007/BF01993560

Twomey, S. (1974). Pollution and the planetary albedo. *Atmospheric Environment*, *8*(12), 1251–1256. https://doi.org/10.1016/0004-6981(74)90004-3

Twomey, S. (1977). The influence of pollution on the shortwave Albedo of clouds. *Journal of the Atmospheric Sciences*, *34*(7), 1149–1152. https://doi.org/10.1175/1520-0469(1977)034<1149:TIOPOT>2.0.CO;2

Virtanen, A., Joutsensaari, J., Kokkola, H., Partridge, D. G., Blichner, S., Seland, Ø., et al. (2025). High sensitivity of cloud formation to aerosol changes. *Nature Geoscience*, *18*(4), 289–295. https://doi.org/10.1038/s41561-025-01662-y

Wang, Y., Fang, F., Li, J., Zhang, P., Ji, Z., Shi, J., & Huang, J. (2025). High effective supersaturation offsets low aerosol hygroscopicity to promote orographic cloud formation over the southern Tibetan Plateau. *npj Climate and Atmospheric Science*, *8*(1), 231. https://doi.org/10.1038/s41612-025-01119-4

Wang, Y., Jia, H., Zhang, P., Fang, F., Li, J., Zhu, L., et al. (2024). Sensitivity of cloud microphysics to aerosol is highly associated with cloud water content: Implications for indirect radiative forcing. *Atmospheric Research*, *309*, 107552. https://doi.org/10.1016/j.atmosres.2024.107552

Wang, Y., Li, J., Fang, F., Zhang, P., He, J., Pöhlker, M. L., et al. (2024). In-situ observations reveal weak hygroscopicity in the Southern Tibetan Plateau: Implications for aerosol activation and indirect effects. *npj Climate and Atmospheric Science*, *7*(1), 77. https://doi.org/10.1038/s41612-024-00629-x

Wang, Y., Niu, S., Lv, J., Lu, C., Xu, X., Wang, Y., et al. (2019). A new method for distinguishing unactivated particles in cloud condensation nuclei measurements: Implications for aerosol indirect effect evaluation. *Geophysical Research Letters*, *46*(23), 14185–14194. https://doi.org/10.1029/2019GL085379

Werner, F., Ditas, F., Siebert, H., Simmel, M., Wehner, B., Pilewskie, P., et al. (2014). Twomey effect observed from collocated microphysical and remote sensing measurements over shallow cumulus. *Journal of Geophysical Research: Atmospheres*, *119*(3), 1534–1545. https://doi.org/10.1002/2013JD020131

Xue, H., & Feingold, G. (2006). Large-eddy simulations of trade wind cumuli: Investigation of aerosol indirect effects. *Journal of the Atmospheric Sciences*, *63*(6), 1605–1622. https://doi.org/10.1175/JAS3706.1

Yang, Y., Zhao, C., Wang, Y., Zhao, X., Sun, W., Yang, J., et al. (2021). Multi-Source data based investigation of aerosol-cloud interaction over the North China Plain and north of the Yangtze Plain. *Journal of Geophysical Research: Atmospheres*, *126*(19), e2021JD035609. https://doi.org/10.1029/2021JD035609

Yuan, T., Li, Z., Zhang, R., & Fan, J. (2008). Increase of cloud droplet size with aerosol optical depth: An observation and modeling study. *Journal of Geophysical Research*, *113*(D4). https://doi.org/10.1029/2007JD008632

Yuan, T., Remer, L. A., Pickering, K. E., & Yu, H. (2011). Observational evidence of aerosol enhancement of lightning activity and convective invigoration. *Geophysical Research Letters*, *38*(4), L04701. https://doi.org/10.1029/2010GL046052

21698996, 2026, 20, Downloaded from https://agupubs.onlinelibrary.wiley.com/doi/10.1029/2026JD046935 by Jianping Huang - Lanzhou University , Wiley Online Library on [10/11/2026]. See the Terms and Conditions (https://onlinelibrary.wiley.com/terms-and-conditions) on Wiley Online Library for rules of use; OA articles are governed by the applicable Creative Commons License

Zhang, P., Wang, Y., Li, J., Fang, F., Zhu, L., & Lv, J. (2025). Improved parameterization of Cloud Droplet spectral dispersion expected to reduce uncertainty in evaluating aerosol indirect effects. *Geophysical Research Letters*, *52*(7), e2024GL111643. https://doi.org/10.1029/2024GL111643

Zhao, C., Qiu, Y., Dong, X., Wang, Z., Peng, Y., Li, B., et al. (2018). Negative aerosol-cloud re relationship from aircraft observations over Hebei, China. *Earth and Space Science*, *5*(1), 19–29. https://doi.org/10.1002/2017EA000346

21698996, 2026, 20, Downloaded from https://agupubs.onlinelibrary.wiley.com/doi/10.1029/2026JD046935 by Jianping Huang - Lanzhou University , Wiley Online Library on [10/11/2026]. See the Terms and Conditions (https://onlinelibrary.wiley.com/terms-and-conditions) on Wiley Online Library for rules of use; OA articles are governed by the applicable Creative Commons License